Journal of Power Sources 196 (2011) 3346–3349

Contents lists available at ScienceDirect

Journal of Power Sources

journal homepage: www.elsevier.com/locate/jpowsour

Short communication

MnO/C core–shell nanorods as high capacity anode materials for lithium-ion batteries

Bing Sun [a], Zhixing Chen [b], Hyun-Soo Kim [c], Hyojun Ahn [d], Guoxiu Wang [a,*]

[a] School of Chemistry and Forensic Science, University of Technology Sydney, Broadway, Sydney, NSW 2007, Australia
[b] School of Mechanical, Materials and Mechatronic Engineering, University of Wollongong, Wollongong, NSW 2522, Australia
[c] Battery Research Centre, Korean Electrotechnology Research Institute, Changwon 641-120, Republic of Korea
[d] School of Materials Science and Engineering, Gyeongsang National University, 900 Gazwa-dong, Jinju, Gyeongnam 660-701, Republic of Korea

ARTICLE INFO

Article history:
Received 4 September 2010
Received in revised form 4 November 2010
Accepted 9 November 2010
Available online 24 November 2010

Keywords:
Core–shell nanostructure
Nanorods
Manganese mono-oxide
Anode materials
Lithium ion batteries

ABSTRACT

MnO/C core–shell nanorods were synthesized by an *in situ* reduction method using MnO_2 nanowires as precursor and block copolymer F127 as carbon source. Field emission scanning electron microscopy and transmission electron microscopy analysis indicated that a thin carbon layer was coated on the surfaces of the individual MnO nanorods. The electrochemical properties were evaluated by cyclic voltammetry and galvanostatic charge–discharge techniques. The as-prepared MnO/C core–shell nanorods exhibit a higher specific capacity than MnO microparticles as anode material for lithium ion batteries.

1. Introduction

Since the first report by Poizot et al., transition metal oxides have attracted great attention as anode materials for lithium ion batteries, due to their high theoretical capacity, safety, low cost, and natural abundance [1–4]. The mechanism for reversible lithium storage is different from the insertion/extraction mechanism in graphite. It involves the reduction and oxidation of metal nanoparticles, accompanying the formation and decomposition of Li_2O, i.e. $MnO_x + 2xLi^+ + e^- \rightarrow M + xLi_2O$. However, there are still many challenges in using them as anode materials for lithium ion batteries. One of them is the poor cycling performance, resulting from large volume expansion during the charge–discharge process due to the generation of Li_2O. Another obstacle is their poor electronic conductivity, which limits their power performance. It has been demonstrated that electrode materials with deliberately designed nanostructure can partly accommodate the strains of Li^+ intercalation and de-intercalation, and the cycling performance can be improved [5]. Furthermore, coating these semiconducting materials with carbon or conductive polymer can significantly enhance the electronic conductivity of the electrode materials, which results in improved rate performance [6–8].

An appropriate anode material should exhibit low voltage vs. Li^+/Li during charge–discharge in order to deliver higher energy density. MnO shows relatively low electromotive force (emf) value (1.032 V vs. Li^+/Li) and high density (5.43 g cm^{-3}) [9,10]. However, this kind of material has seldom been reported as an anode material. Recently, Li's group has reported nanocrystalline MnO thin film, and MnO powder as anode has shown low overpotential and good cycling performance [11,12]. Liu et al. also synthesised MnO/C nanocomposite by thermal decomposition of manganese benzoate precursor at 500 °C under air atmosphere [13]. In this paper, we report the synthesis of MnO/C core–shell nanorod electrode material and investigate its electrochemical performance as anode material for lithium ion batteries. The prepared MnO/C core–shell nanorods showed much higher specific capacity than that of MnO microparticles and MnO_2 nanowires as anode material of lithium ion battery.

2. Experiment

MnO/C core–shell nanorods were synthesized by the reduction of carbon precursor coated MnO_2 nanowires. The MnO_2 nanowires were synthesized by a typical hydrothermal reaction according to previously reported procedures [14]. 0.7 mmol $KMnO_4$ and 0.7 mmol NH_4Cl were dissolved in 35 ml distilled water to form a transparent solution under stirring. The solution was sealed in a Teflon-lined stainless steel autoclave and kept at 140 °C for

* Corresponding author. Tel.: +61 2 95141741; fax: +61 2 95141717.
E-mail address: Guoxiu.Wang@uts.edu.au (G. Wang).

0378-7753/$ – see front matter © 2010 Elsevier B.V. All rights reserved.
doi:10.1016/j.jpowsour.2010.11.090

24 h. After cooling down to room temperature, the precipitate was collected by filtration and rinsed with distilled water and absolute alcohol several times, and then dried in vacuum oven at 60 °C overnight. Non-ionic block co-polymer poly (ethylene oxide)-*block*-poly (propylene oxide)-*block*-poly (ethylene oxide) ($EO_{106}PO_{70}EO_{106}$) Pluronic®F127 (Sigma–Aldrich) was used as the carbon precursor for carbon coating in this work. 29 mg F127 was first dissolved in 10 ml ethanol to form a transparent solution. Then, 56 mg MnO_2 nanowires were added to the solution and ultrasonicated for 30 min in a sealed bottle. After drying under stirring at room temperature, the product was ground into powder and sintered at 500 °C for 5 h in flowing Ar containing 5 vol.% H_2.

The crystal structure of the as-prepared materials was characterized by X-ray diffraction (XRD, GBC MMA) using Cu Kα radiation, with 2θ ranging from 10° to 80°. Field emission scanning electron microscopy (FESEM, JEOL 7500) and transmission electron microscopy (TEM, JEOL 2011) were used to investigate the morphology of the as-prepared materials. The electrochemical experiments were performing using 2032 coin-type cells assembled in an argon-filled glove box. The working electrodes were fabricated by using a mixed slurry of active materials (70 wt%), acetylene black (20 wt%), and polyvinylidene fluoride (PVDF 10 wt%) in *N*-methyl-2-pyrrolidone (NMP). The slurry was spread onto the Cu foil with a doctor blade and dried at 120 °C overnight under vacuum. The electrode area is 1 cm^2 and the loading of active material is 1.0–1.2 mg cm^{-2}. The electrolyte consisted of a solution of 1 M $LiPF_6$ in ethylene carbonate (EC) and dimethyl carbonate (DMC) with a weight ratio of 1:1 (Zhangjiagang Guotaihuarong Ltd., H_2O < 20 ppm). Pure lithium foil was used as counter and reference electrode. Cyclic voltammetry (CV) measurement of the cells were carried out using a CHI660C electrochemical workstation. Charge–discharge testing was performed in the range of 0.01–3.0 V on a computer-controlled Land Battery Testing system. The specific capacity was calculated based on the weight of the MnO/C composite.

3. Results and discussion

The MnO/C core–shell nanorods were prepared by *in situ* reduction of MnO_2 nanowires with carbon coating. In the first step, MnO_2 nanowires were synthesized by hydrothermal reaction. The crystal structure of the as-prepared MnO_2 nanowires was confirmed by XRD (Fig. 1). All the diffraction peaks can be indexed to the body-centered tetragonal α-MnO_2 phase (JCPDS 44-0141). In the second step, MnO/C core–shell nanorods were obtained through

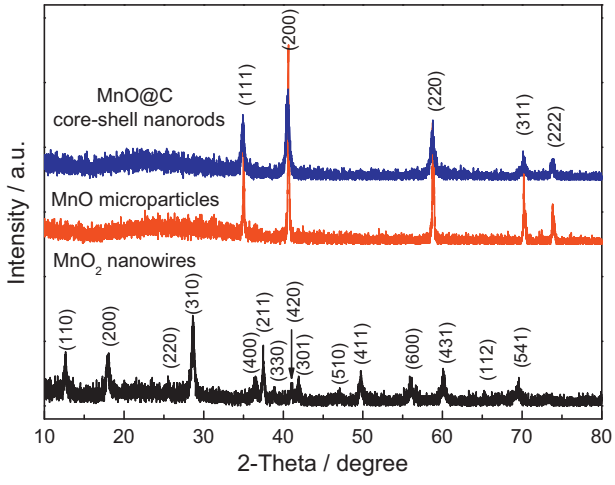

Fig. 1. X-ray diffraction patterns of the as-prepared MnO/C core–shell nanorods and MnO_2 nanowires.

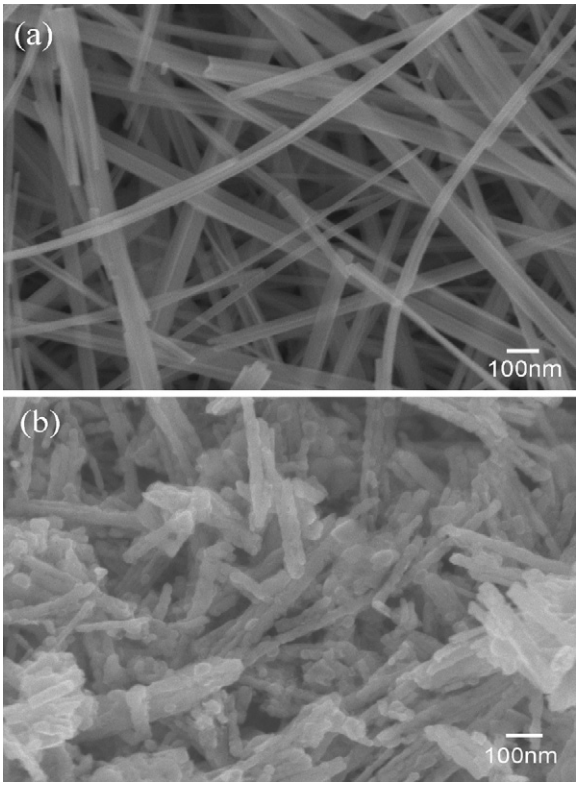

Fig. 2. FESEM images of (a) MnO_2 nanowires (b) MnO/C core–shell nanorods.

sintering the carbon precursor coated MnO_2 nanowires in flowing Ar containing 5 vol.% H_2. As shown in Fig. 1, the crystal structure of MnO/C core–shell nanorods can be indexed to the face-centered cubic phase of MnO (JCPDS 07-0230). The broad, low intensity diffraction peak in the range of 20–30° is likely associated with the presence of amorphous carbon, which is originated from the decomposition of the copolymer surfactant.

The morphologies of the as-prepared materials were observed by FESEM and shown in Fig. 2. The as-prepared MnO_2 shows nanowire structure with diameters ranging from 20–50 nm (Fig. 2(a)). After reducing to MnO during the sintering process, the nanowire structures fractured into nanorods (Fig. 2(b)). There is no significant change in diameter. More structural details of the MnO/C nanorods were further analyzed by TEM, high resolution TEM (HRTEM) and selected area electron diffraction (SAED). Low magnification TEM images are shown in Fig. 3(a) and (b). The nanorods show polycrystalline feature and are agglomerated into bundles with a length extending to a few hundred nanometers. The fracturing of the nanowire structure into nanorods may be caused by the reduction from MnO_2 to MnO. An individual nanorod consists of nanoparticles with diameters from 20 nm to 30 nm. The corresponding SAED pattern is shown as the inset in Fig. 3(b). All the diffraction rings can be indexed to the face-centered cubic Fm-3m crystal structure. A HRTEM image is presented in Fig. 3(c). In the region A, we can clearly observe that the image is in focus on the surface of the MnO crystal, and the lattice can be clearly resolved with a d-spacing of 0.255 nm for the (1 1 1) planes. However, in the region B at the same level, the image is focused on the carbon layer, which presents numerous black spots, indicating that the surface of the nanorod is covered with a thin layer of amorphous carbon. On the edge of the nanorod, a thin carbon layer with a thickness of 1–2 nm is clearly visible.

The electrochemical behavior of the prepared MnO/C nanorods was initially characterized by cyclic voltammetry (CV), as shown in Fig. 4. In the negative scan process, two small peaks appeared

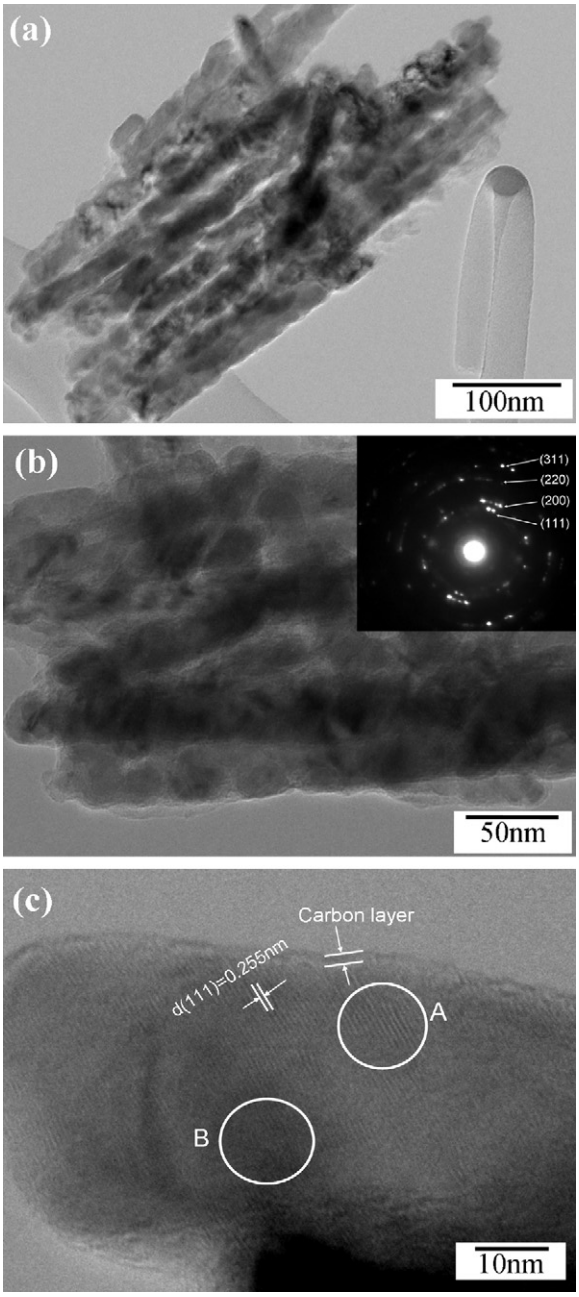

Fig. 3. (a and b) TEM images of MnO/C core–shell nanorods, with the inset in (b) showing the corresponding SAED pattern, and (c) HRTEM image of MnO/C core–shell nanorods.

at 1.86 V and 1.53 V, and disappeared in the subsequent cycles. These reduction peaks may correspond to the reduction of Mn^{3+} or Mn^{4+} to Mn^{2+}, which could be originated from trace MnO_{1+x} impurity from the incomplete reduction of MnO_2 in the sintering process. The main cathodic peak is close to 0.1 V, corresponding to the complete reduction of Mn^{2+} to Mn^0 and the formation of a solid electrolyte interphase (SEI) layer with a reversible polymer/gel like film [15,16]. From the second cycle, the reduction current peaks shift to 0.3 V, indicating an irreversible phase transformation due to the formation of Li_2O and metallic manganese. In the anodic polarization process, one main peak appeared at around 1.3 V, and a weak peak was recorded at 2.1 V, corresponding to the oxidation of Mn^0 to Mn^{2+} and the decomposition of the polymer/gel layer at high oxidation potential above 2.0 V [15]. After the second cycle, the CV curves become stable and overlap.

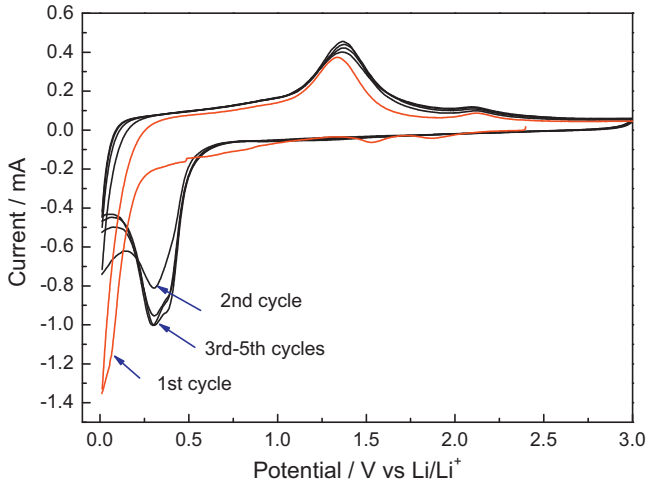

Fig. 4. Cyclic voltammetry (CV) curves of MnO/C core–shell nanorod electrode. Scanning rate: 0.2 mV s^{-1} in the range of 0.01–3.0 V.

The electrochemical performances were further investigated by charge–discharge measurements with cycling at a current density of 200 mA g^{-1} between 0.01 and 3.0 V at ambient temperature. In the first discharge curve of MnO/C core–shell nanorods shown in Fig. 5(a), the voltage dropped quickly to a plateau about 0.28 V, and then decreased slowly to 0.01 V, associated with the complete

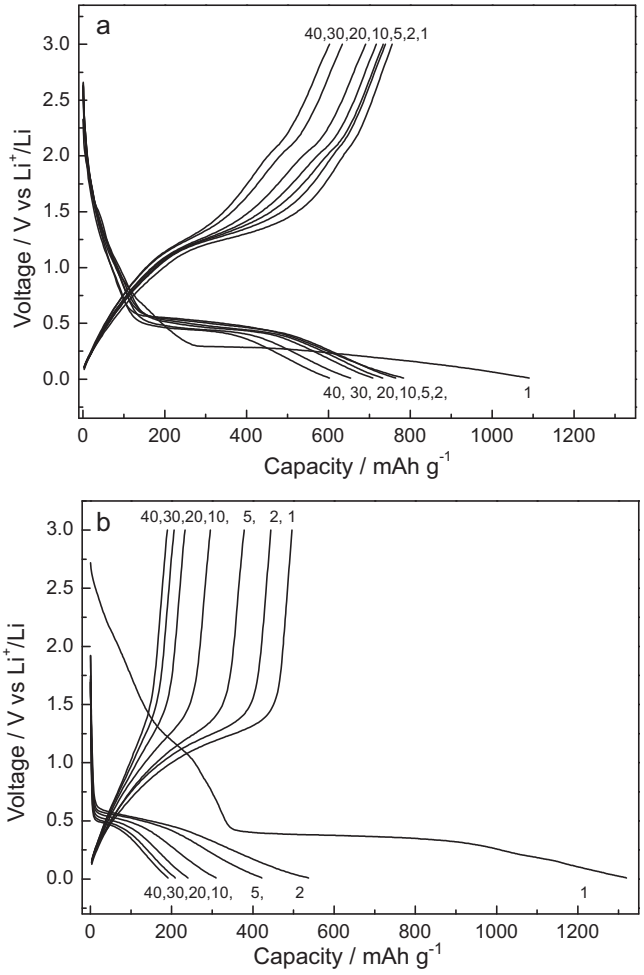

Fig. 5. Voltage profiles of the electrode made of as-prepared (a) MnO/C core–shell nanorods, and (b) MnO_2 nanowires. Current density: 200 mA g^{-1}.

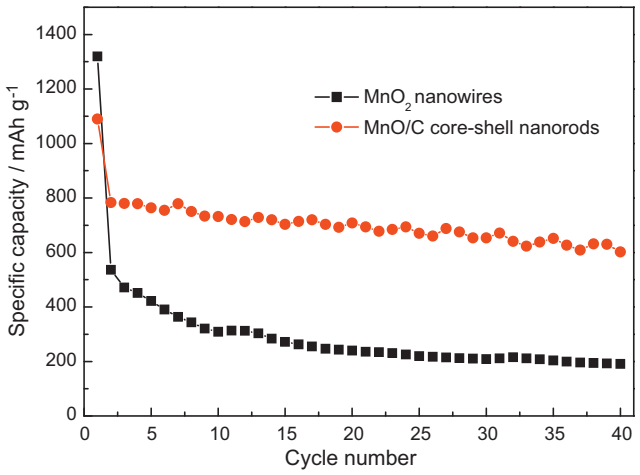

Fig. 6. Cycling performance of MnO_2 nanowire and MnO/C core–shell nanorod electrodes at discharge and charge current rate of 200 mA g^{-1}.

reduction of Mn^{2+} to Mn^0. For the initial charge curve, the electrode shows a slope in the voltage range between 1.0 and 1.5 V, related to the oxidation of Mn^0 to Mn^{2+}. The voltage plateau for this reaction should be at the emf value of 1.032 V vs. Li^+/Li at 298 K for perfect bulk materials [9,10]. The difference in the plateau position is considered to be caused by the cathodic overpotential, which has already been studied by Zhong et al. using the galvanostatic intermittent titration technique (GITT) [12]. The voltage profiles of MnO_2 nanowires are similar to MnO/C core–shell nanorods except for the position of the charge–discharge plateau (Fig. 5(b)). The initial discharge capacities of the MnO/C nanorods and MnO_2 nanowires are 1090 mAh g^{-1} and 1319 mAh g^{-1}, respectively, which are larger than their theoretical capacities. The theoretical capacity for MnO_2 is 1232 mAh g^{-1} and MnO has a theoretical capacity of 755 mAh g^{-1}. The exceeding capacities could be ascribed to the decomposition of the electrolyte at low voltage (generally below 0.8 V vs Li^+/Li) to form a solid electrolyte interphase (SEI) layer and further lithium storage *via* interfacial charging at metal/Li_2O interface [17]. As shown in Fig. 5 (a), the discharge plateau of MnO/C nanorod electrode has shifted to about 0.5 V from the second cycle, indicating the irreversible formation of crystalline metal nanoparticles and amorphous Li_2O matrix. The long cycling performance results of MnO/C nanorod and MnO_2 nanowires electrodes are shown in Fig. 6. The MnO/C core–shell nanorod electrode exhibited higher capacity than that of MnO_2 nanowire electrode after 40 cycles. The good electrochemical performance of MnO/C core–shell nanorods is a result of the combined advantages of the nanorod structure and the porous carbon coating layer. Nanosize materials with large surface area can provide more active sites for Li^+ intercalation/de-intercalation and shorten the diffusion length for lithium ions in the solid phase. The nanoporous carbon coating layer with mesopores can form a mixed conducting 3D network that facilitates the migration of both the Li^+ and the e^-, so that they reach each surface of the MnO nanorods [18].

4. Conclusions

Using block copolymer F127 as the carbon source, MnO/C core–shell nanorods were successfully prepared from MnO_2 nanowires by calcination in a gas flow of 5 vol.% H_2 in Ar. The XRD pattern shows that the product has a face-centered cubic phase structure. FESEM and TEM images show that a thin carbon layer was coated on the surfaces of the MnO nanorods. The MnO/C core–shell nanorod electrodes delivered a higher specific discharge capacity than MnO_2 nanowires after 40 cycles. However, MnO/C core–shell nanorods, despite having improved specific capacity relative to graphite, have comparably low cyclability relative to graphite. Further improvements are required for potential application as an alternative anode material in lithium ion batteries.

Acknowledgements

This project is financially supported by Australian Research Council (ARC) through the ARC Linkage project (LP0989134), BEZEL New Energy Science and Technology Co., Ltd., and Daejung Energy Materials Co., Ltd. We also acknowledge the support from the National Foundation of Korea through the WCU (World Class University) Program (R32-2008-000-20093-0).

References

[1] P. Poizot, S. Laruelle, S. Grugeon, L. Dupont, J.M. Tarascon, Nature 407 (2000) 496.
[2] F. Jiao, P.G. Bruce, Adv. Mater. 19 (2007) 657.
[3] A.L.M. Reddy, M.M. Shaijumon, S.R. Gowda, P.M. Ajayan, Nano Lett. 9 (2009) 1002.
[4] M.S. Wu, P.C.J. Chiang, J.T. Lee, J.C. Lin, J. Phys. Chem. B 109 (2005) 23279.
[5] L. Wang, H.W. Xu, P.C. Chen, D.W. Zhang, C.X. Ding, C.H. Chen, J. Power Sources 193 (2009) 846.
[6] L.W. Ji, X.W. Zhang, Electrochem. Commun. 11 (2009) 795.
[7] W.M. Zhang, X.L. Wu, J.S. Hu, Y.G. Guo, L.J. Wan, Adv. Funct. Mater. 18 (2008) 3941.
[8] H. Liu, G.X. Wang, J.Z. Wang, D. Wexler, Electrochem. Commun. 10 (2008) 1879.
[9] P. Poizot, S. Laruelle, S. Grugeon, J.M. Tarascon, J. Electrochem. Soc. 149 (2002) A1212.
[10] H. Li, P. Balaya, J. Maier, J. Electrochem. Soc. 151 (2004) A1878.
[11] X.Q. Yu, Y. He, J.P. Sun, K. Tang, H. Li, L.Q. Chen, X.J. Huang, Electrochem. Commun. 11 (2009) 791.
[12] K.F. Zhong, X. Xia, B. Zhang, H. Li, Z.X. Wang, L.Q. Chen, J. Power Sources 195 (2010) 3300.
[13] J. Liu, Q.M. Pan, Electrochem. Solid-State Lett. 13 (2010) A139.
[14] Y.Q. Gao, Z.G. Wang, J.X. Wan, G.F. Zou, Y.T. Qian, J. Cryst. Growth 279 (2005) 415.
[15] M.S. Wu, P.C.J. Chiang, J.T. Lee, J.C. Lin, J. Phys. Chem. B. 109 (2005) 23279.
[16] S. Laruelle, S. Grugeon, P. Poizot, M. Dolle, L. Dupont, J.M. Tarascon, J. Electrochem. Soc. 149 (2002) A627.
[17] J. Jamnik, J. Maier, Phys. Chem. Chem. Phys. 5 (2003) 5215.
[18] X.L. Wu, L.Y. Jiang, F.F. Cao, Y.G. Guo, L.J. Wan, Adv. Mater. 21 (2009) 2710.